




Non-local electrical spin injection and detection in germanium at room temperature

Cite as: Appl. Phys. Lett. **111**, 182401 (2017); <https://doi.org/10.1063/1.5003244>

Submitted: 04 September 2017 . Accepted: 20 October 2017 . Published Online: 31 October 2017

F. Rortais, C. Vergnaud , A. Marty , L. Vila, J.-P. Attané, J. Widiez, C. Zucchetti, F. Bottegoni, H. Jaffrès , J.-M. George, and M. Jamet



View Online



Export Citation



CrossMark

ARTICLES YOU MAY BE INTERESTED IN

[Conversion of spin current into charge current at room temperature: Inverse spin-Hall effect](#)
Applied Physics Letters **88**, 182509 (2006); <https://doi.org/10.1063/1.2199473>

[Investigation of spin scattering mechanism in silicon channels of Fe/MgO/Si lateral spin valves](#)

Applied Physics Letters **110**, 192401 (2017); <https://doi.org/10.1063/1.4982966>

[Spin diffusion length of Permalloy using spin absorption in lateral spin valves](#)
Applied Physics Letters **111**, 082407 (2017); <https://doi.org/10.1063/1.4990652>



**THE WORLD'S RESOURCE FOR
VARIABLE TEMPERATURE
SOLID STATE CHARACTERIZATION**



WWW.MMR-TECH.COM

OPTICAL STUDIES SYSTEMS

SEEBECK STUDIES SYSTEMS

MICROPROBE STATIONS

HALL EFFECT STUDY SYSTEMS AND MAGNETS

Non-local electrical spin injection and detection in germanium at room temperature

F. Rortais,¹ C. Vergnaud,¹ A. Marty,¹ L. Vila,¹ J.-P. Attané,¹ J. Widiez,² C. Zucchetti,³
 F. Bottegoni,³ H. Jaffrès,⁴ J.-M. George,⁴ and M. Jamet¹

¹Spintec, Institut Nanosciences et Cryogénie, Univ. Grenoble Alpes, CEA, CNRS, F-38000 Grenoble, France

²CEA, LETI, MINATEC Campus, F-38054 Grenoble, France

³LNES-Dipartimento di Fisica, Politecnico di Milano, 20133 Milano, Italy

⁴Unité Mixte de Physique, CNRS, Thales, Univ. Paris-Sud, Univ. Paris-Saclay, 91767 Palaiseau, France

(Received 4 September 2017; accepted 20 October 2017; published online 31 October 2017)

Non-local carrier injection/detection schemes lie at the very foundation of information manipulation in integrated systems. This paradigm consists in controlling with an external signal the channel where charge carriers flow between a “source” and a well separated “drain.” The next generation electronics may operate on the spin of carriers in addition to their charge and germanium appears as the best hosting material to develop such a platform for its compatibility with mainstream silicon technology and the predicted long electron spin lifetime at room temperature. In this letter, we demonstrate injection of pure spin currents (i.e., with no associated transport of electric charges) in germanium, combined with non-local spin detection at 10 K and room temperature. For this purpose, we used a lateral spin valve with epitaxially grown magnetic tunnel junctions as spin injector and spin detector. The non-local magnetoresistance signal is clearly visible and reaches ≈ 15 m Ω at room temperature. The electron spin lifetime and diffusion length are 500 ps and 1 μ m, respectively, the spin injection efficiency being as high as 27%. This result paves the way for the realization of full germanium spintronic devices at room temperature. *Published by AIP Publishing.*

<https://doi.org/10.1063/1.5003244>

Spintronics aim at exploiting the spin degree of freedom to manipulate information, while in conventional electronics, information is associated with the charge of carriers.^{1–3} In this regard, *n*-type germanium appears as the best hosting material for spin transport and manipulation.^{4,5} The electron spin lifetime is predicted to reach several nanoseconds at room temperature⁶ and the compatibility with mainstream silicon technology allows exploiting the spin-related properties of low dimensional SiGe-heterostructures.⁷ Electrical spin injection and detection has been explored in Ge films or nanowires using either non-local (NL) measurements in lateral spin valve (LSV) or vertical spin valves^{8–11} or the Hanle effect in three-terminal devices.^{12–19} So far, the non-local lateral geometry is the most interesting one for the development of spintronics since the spin can be manipulated in the Ge channel between the spin injector and detector. However, experimental measurements have been limited in temperature to 225 K (Ref. 8) and the only demonstration at room temperature used an indirect method based on the combination of spin pumping and inverse spin Hall effect (ISHE).²⁰

Here, we demonstrate the lateral spin transport in *n*-type germanium-on-insulator (GeOI, $n = 2 \times 10^{19}$ cm⁻³) at 10 K and room temperature using lateral spin valves. By performing non-local magnetoresistance, Hanle and oblique Hanle effect measurements, we could accurately extract the spin lifetime, spin diffusion length, and spin injection efficiency to be ($\tau_{sf} = 750$ ps; $l_{sf} = 1.5$ μ m; $\langle P \rangle = 10\%$) and ($\tau_{sf} = 500$ ps; $l_{sf} = 1$ μ m; $\langle P \rangle = 27\%$) at 10 K and room temperature, respectively. The weak dependence of the spin lifetime with temperature is in agreement with a spin relaxation dominated

by spin scattering on ionized dopants and the Elliott-Yafet mechanism.

For electrical spin injection and detection, we use lateral spin valves (LSVs) fabricated on GeOI. The Ge layer is 1 μ m-thick with uniform *n*-type heavy doping ($n = 2 \times 10^{19}$ cm⁻³) to favor electrical conduction and reduce the width of the Schottky barrier. The SiO₂ buried oxide layer (BOX) is also 1 μ m-thick. GeOI was used to well-define the conduction channel and it was fabricated using the Smart CutTM process from Ge epitaxially grown on Si at low temperature (400 °C).²¹ By using short duration thermal cycling under H₂ atmosphere, the threading dislocation density was reduced down to 10⁷ cm⁻². However, a residual tensile strain of +0.148% (as determined by grazing incidence x-ray diffraction) built up during the cooling-down to room temperature after the thermal cycling due to the difference of thermal expansion coefficients between Ge and Si. The Ge layer is protected against oxidation by a 10 nm-thick SiO₂ film which is removed using hydrofluoric acid before the introduction into the molecular beam epitaxy (MBE) chamber. The native Ge oxide top layer was then thermally removed by annealing under ultrahigh vacuum. After this cleaning procedure, the reflection high-energy electron diffraction (RHEED) pattern exhibited a well-defined and high-quality (2 \times 1) surface reconstruction as the one shown in Fig. 1(a). To achieve electrical spin injection and detection, we used MgO-based magnetic tunnel junctions (MTJ) to avoid the impedance mismatch issue.²² Moreover, in order to reduce the density of localized states at the MgO/Ge interface,^{15,23} we have grown the magnetic tunnel junction Pd(5 nm)/Fe(15 nm)/MgO(2.5 nm) by epitaxy on Ge(100). The overall epitaxial relationship is Fe[100]||MgO[110]||Ge[100] as illustrated by

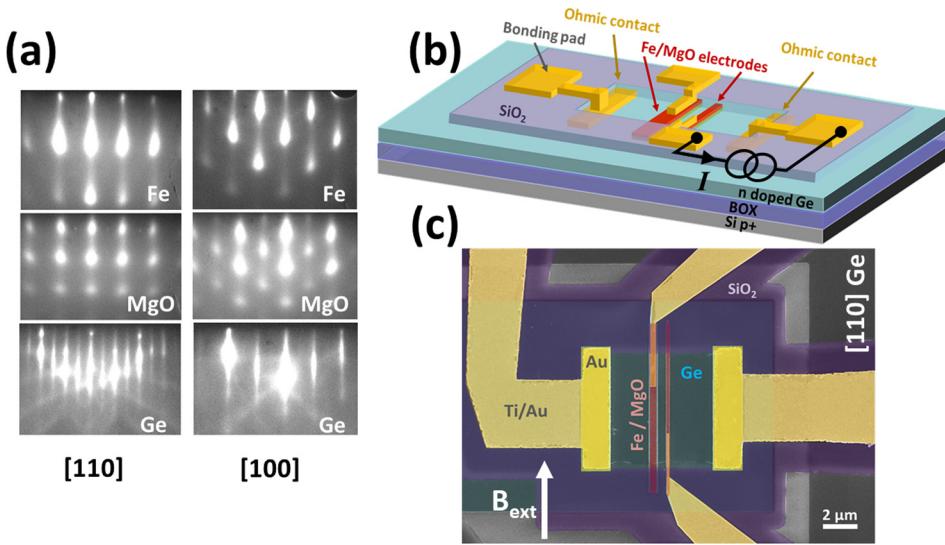


FIG. 1. (a) RHEED patterns recorded along the [110] and [100] crystal axes of Ge at different stages of the epitaxial growth of the magnetic tunnel junction on Ge(100). (b) Sketch of the lateral spin valve used for non-local electrical spin injection and detection in *n*-Ge. The electrical current is applied between the hard magnetic layer and one ohmic contact in electron spin injection conditions. (c) Scanning electron microscopy image of the lateral spin valve.

the RHEED patterns along the [110] and [100] crystal axes of Ge in Fig. 1(a). The sample is then processed into LSVs made of two magnetic tunnel junctions and two ohmic contacts as schematically shown in Fig. 1(b). The nanofabrication process required 5 successive electron beam lithography levels and the key steps are: (i) the ion beam etching of the ferromagnetic electrodes using metallic hard masks, (ii) the growth of ohmic contacts made of Au(250 nm)/Ti(10 nm) by electron beam evaporation and lift-off technique, and (iii) the deposition of a 100 nm-thick SiO₂ passivation layer by ion beam deposition (IBD) to insulate the bonding pads from the Ge channel. An example of LSV is shown in Fig. 1(c) where the gap, defined as the distance between the ferromagnetic electrodes edges, is 0.5 μm. The soft and hard magnetic electrodes have been processed with their long axis either along the [110] or the [100] Ge crystal axes and their dimensions are 1 × 20 μm² and 0.5 × 20 μm², respectively. The external magnetic field **B**_{ext} has always been applied along the [110] Ge crystal axis as shown in Fig. 1(c) which corresponds to the hard magnetic axis of Fe electrodes. The MTJs *I*(*V*) curves are almost linear and their resistance-area product ranges between 100 and 600 Ω μm². Magnetoresistance measurements were performed on device A (gap 1 μm) at 10 K and on device B (gap 0.2 μm) at 295 K. We could not perform full temperature dependence on a single device because contact pads degraded when ramping the temperature. Measurements could be repeated on 5 different lateral spin valves on the same chip with different gaps between the two MTJs.

The measurement configuration of Figs. 2 and 3 is the non-local (NL) geometry as schematically shown in the top panel of Figs. 2(a) and 3(a): the current is applied between one pair of ferromagnetic-ohmic contacts and the voltage measured on the other pair. By this, only a pure spin current flows between the two ferromagnets without any charge current avoiding the contribution from spurious tunneling magnetoresistance effects to the detected signal.^{24,25} Moreover, in the non-local geometry, we cannot detect any spin signal amplification due to spin accumulation into interface states like in three-terminal measurements.²³ The measured magnetoresistance signal is $\Delta R_{NL} = R_{\downarrow\downarrow} - R_{\uparrow\uparrow} \approx -1.7 \text{ m}\Omega$ on device A at 10 K applying a DC of 20 mA and $\Delta R_{NL} = R_{\downarrow\downarrow} - R_{\uparrow\uparrow} \approx -14 \text{ m}\Omega$ on

device B at 295 K applying a DC of 2 mA. At both 10 K and 295 K, the NL voltage exhibits a linear dependence on the applied DC as shown in Figs. 2(b) and 3(b), respectively. Only a saturation behavior is observed at high currents and 10 K as already observed by Sasaki *et al.* in silicon and which is likely due to the reduction of the tunneling spin injection at high bias voltages.²⁶ In Figs. 2(c) and 3(c), the corresponding spin resistance signals ΔR_{NL} are then almost constant with the applied DC. This bias dependence is different from that obtained by Zhou *et al.* who observed a strong spin signal asymmetry with respect to zero bias.⁸ However, this asymmetry was explained by the non-uniform doping profile of the Ge film whereas, in our case, the Ge film is uniformly doped at $2 \times 10^{19} \text{ cm}^{-3}$ on the 1 μm-thick.

Since the MTJ resistance-area product is 2 orders of magnitude larger than $r_{Ge} = \rho \times l_{sf}$, ρ and l_{sf} being the Ge

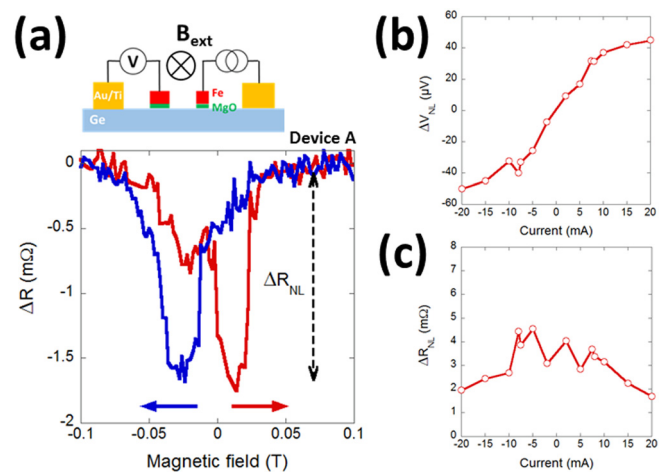


FIG. 2. (a) Schematics of the non-local measurement geometry and non-local magnetoresistance measurements at 10 K on device A. The gap between the 2 MTJs is 1 μm. The applied DC I_{DC} is 20 mA in electron spin injection conditions. The magnetic field is applied in-plane along the Fe electrodes, i.e., along the Ge [110] crystal direction as shown in Fig. 1(c). The horizontal arrows indicate the field sweep directions. Red (resp. blue) is for increasing (resp. decreasing) magnetic field. Both curves have been shifted vertically so that the high field magnetoresistance ΔR is zero. (b) and (c) Bias current dependence of the non-local voltage $\Delta V_{NL} = \Delta R_{NL} \times I_{DC}$ and non-local magnetoresistance ΔR_{NL} at 10 K, respectively.

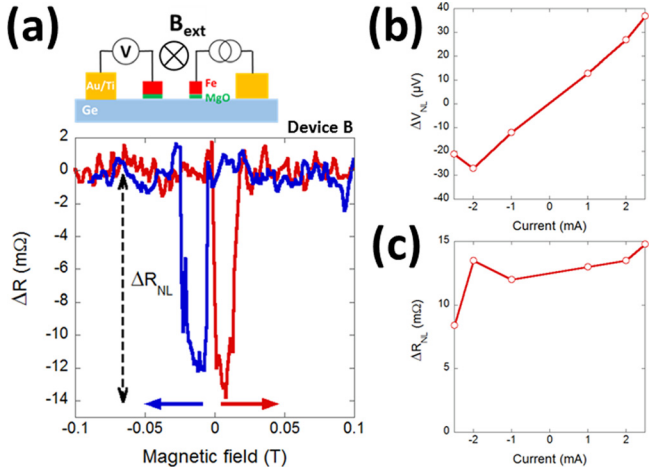


FIG. 3. (a) Schematics of the non-local measurement geometry and non-local magnetoresistance measurements at 295 K on device B. The gap between the 2 MTJs is $0.2 \mu\text{m}$. The applied DC I_{DC} is 2 mA in electron spin injection conditions. The magnetic field is applied in-plane along the Fe electrodes, i.e., along the Ge [110] crystal direction as shown in Fig. 1(c). The horizontal arrows indicate the field sweep directions. Red (resp. blue) is for increasing (resp. decreasing) magnetic field. Both curves have been shifted vertically so that the high field magnetoresistance ΔR is zero. (b) and (c) Bias current dependence of the non-local voltage $\Delta V_{NL} = \Delta R_{NL} \times I_{DC}$ and non-local magnetoresistance ΔR_{NL} at 295 K, respectively.

resistivity and the predicted spin diffusion length, the non-local spin signal can be written as²⁷

$$\Delta R_{NL} = -\frac{\rho P_I P_D}{A} l_{sf} \exp\left(-\frac{L}{l_{sf}}\right), \quad (1)$$

where P_I (resp. P_D) is the spin polarization of the tunnel current at the injection (resp. detection) electrode and A the cross-sectional area of the Ge channel. L is the distance between the centers of the ferromagnetic electrodes (i.e., the gap plus half the width of each electrode) and l_{sf} the spin diffusion length in Ge. In principle, Eq. (1) should be multiplied by a factor: $\frac{4l_{sf}^2 \sinh(\frac{w_1}{2l_{sf}}) \sinh(\frac{w_2}{2l_{sf}})}{w_1 w_2}$ to take into account the fact that spin injection and detection spread over the electrodes widths w_1 and w_2 . In our case, the spin diffusion length is of the order of magnitude of the electrodes widths and this factor is only a few percent above 1. For instance, it is 1.05 for $l_{sf} = 1 \mu\text{m}$. Hence, we do not consider this factor in the following.

In order to estimate l_{sf} and deduce the $P_I P_D$ product, we have performed Hanle and oblique Hanle measurements where the external magnetic field is not collinear to the injected spin direction inducing spin precession and dephasing. The measurements are summarized in Fig. 4. In the Hanle geometry [Fig. 4(a) for device A and Fig. 4(b) for device B], the external field is applied perpendicular to the film plane, i.e., perpendicular to the injected spin direction. In the oblique Hanle geometry [Fig. 4(c) for device C with a gap of $2 \mu\text{m}$], the external field is applied in the film plane at 45° with respect to the magnetic electrode long axis, i.e., at 45° from the injected spin direction. In both geometries, injected spins experience the Larmor precession and the spin signal ΔR_{NL}^{Hanle} decays following roughly a Lorentzian curve. Starting from the parallel state, the spin signal can be written as²⁷

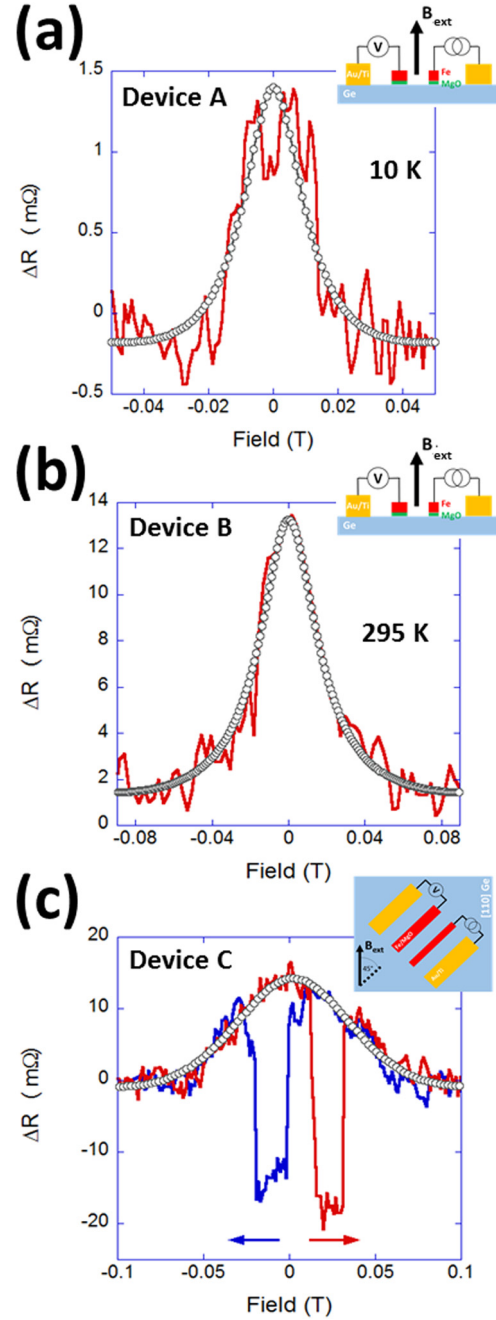


FIG. 4. (a) and (b) Hanle measurements with the applied magnetic field perpendicular to the Ge film at 10 K on device A and at 295 K on device B, respectively. The applied DC I_{DC} is 3 mA and 5 mA in electron spin injection conditions. The red solid lines are experimental data, and black open dots are fits using Eq. (2). The gaps are $1 \mu\text{m}$ and $0.2 \mu\text{m}$, respectively. The initial magnetic state is the parallel state. (c) Oblique Hanle measurements on device C at 295 K. The magnetic field is applied along the [110] Ge crystal axis at 45° with respect to the Fe electrodes long axis. The applied DC is 10 mA in electron spin injection conditions. The gap is $2 \mu\text{m}$.

$$\Delta R_{NL}^{Hanle}(B_{ext}) \propto \int_0^\infty P(t) f(t) \exp\left(-\frac{t}{\tau_{sf}}\right) dt, \quad (2)$$

where $P(t) = [1/\sqrt{4\pi Dt}] \exp[-L^2/(4Dt)]$ is the diffusion function and D the electron diffusion coefficient we determined independently using double Hall crosses: $D = 32 \pm 3 \text{ cm}^2 \text{ s}^{-1}$ at 10 K and $23 \pm 2 \text{ cm}^2 \text{ s}^{-1}$ at 295 K. $f(t) = \cos(\omega_L t)$ for the Hanle effect and $f(t) = (1 + \cos(\omega_L t))/2$ for the oblique Hanle effect at 45° both reflecting the spin

precession, $\omega_L = g\mu_B B_{ext}/\hbar$ is the Larmor angular frequency with g , the g -factor of electrons in the Ge conduction band, μ_B the Bohr magneton, and \hbar the reduced Planck's constant. τ_{sf} is the electron spin lifetime in Ge. By fitting the Hanle curves at 10 K and 295 K in Figs. 4(a) and 4(b) using the analytical solution of Eq. (2) (Refs. 28 and 29) and $g = 1.54$,³⁰ we find $\tau_{sf} = 750 \pm 100$ ps, $l_{sf} = \sqrt{D\tau_{sf}} = 1.5 \pm 0.2 \mu\text{m}$ at 10 K and $\tau_{sf} = 500 \pm 50$ ps, $l_{sf} = 1.0 \pm 0.1 \mu\text{m}$ at 295 K. The spin diffusion length at room temperature is close to that obtained by Dushenko *et al.*²⁰ who found $l_{sf} = 0.66 \pm 0.2 \mu\text{m}$ in a Ge film with comparable n -type doping by non-local spin pumping. This value is also in good agreement with that obtained by three-terminal measurements at room temperature: $1.3 \mu\text{m}$ for $n = 10^{18} \text{cm}^{-3}$ (Ref. 15) and $0.53 \mu\text{m}$ for $n = 1.0 \times 10^{19} \text{cm}^{-3}$.¹⁷ This agreement between non-local and three-terminal Hanle measurements can be attributed to the fact that interface states are only weakly confined at room temperature and have little influence on the spin injection mechanism¹⁵ which might not be the case at low temperature. We notice that the spin lifetime only decreases by a factor 1.5 between 10 K and 295 K. This little temperature dependence is expected for donor-driven spin relaxation in multi-valley semiconductors like Ge at high doping levels (here $2 \times 10^{19} \text{cm}^{-3}$).^{31,32} In Fig. 4(c), the magnetoresistance signal obtained in the oblique Hanle configuration looks very similar to that obtained by Li *et al.* using spin-polarized ballistic hot electron injection and detection¹¹ in intrinsic Ge. In their case, the spin signal decay is attributed to a reminiscent Dyakonov-Perel mechanism due to the g -factor anisotropy in Ge. The spin scattering rate associated to this spin relaxation process adds to the Elliott-Yafet mechanism and can be written as $1/\tau_{s,B} = \eta \zeta \frac{\omega_L^2 \tau_m}{1 + \omega_L^2 \tau_m^2}$.³³ $\eta = (\alpha^4 + \beta^4 + \gamma^4)$ with α , β , and γ are the directional cosines of the external applied field \mathbf{B}_{ext} with respect to the Ge lattice coordinates, $\zeta = 2[(g_{\parallel} - g_{\perp})/(g_{\parallel} + 2g_{\perp})]^2 \approx 0.11$ relates to the g -factor anisotropy and τ_m is the electron momentum relaxation time. In our highly doped Ge film, we can consider the following electron momentum relaxation times at 295 K: $\tau_{m,imp} \approx 200$ fs for electron scattering on ionized dopants and $\tau_{m,ph} \approx 450$ fs for electron intervalley scattering with phonons.³⁴ The resulting momentum relaxation time is $\tau_m \approx 140$ fs which gives $1/\tau_{s,B} \approx 10^6 \text{s}^{-1}$ for a maximum applied magnetic field of 0.1 T. Hence, the spin relaxation rate due to the g -factor anisotropy is more than 3 orders of magnitude smaller than the spin relaxation rate due to the Elliott-Yafet mechanism on ionized dopants and can be considered as negligibly small in our system. This result is consistent with a Dyakonov-Perel mechanism where the spin relaxation rate is inversely proportional to the electron momentum relaxation rate. Therefore, the spin signal decay in the oblique Hanle geometry is only due to spin precession. However, by fitting the oblique Hanle effect signal using Eq. (2) and $g = 1.54$ at room temperature, we obtain $\tau_{sf} \approx 50$ ps which is one order of magnitude less than the value deduced from Hanle measurements. First, we have verified, by numerical simulations, that the rotation of the electrodes magnetization along the applied field cannot justify this shorter spin lifetime. In order to reproduce the experimental data, we use the g -factor as a free parameter and obtain $\tau_{sf} = 350 \pm 150$ ps, $l_{sf} = 0.9 \pm 0.2 \mu\text{m}$,

and $g = 0.7 \pm 0.2$. τ_{sf} and l_{sf} are now in agreement with those obtained by Hanle measurements, but the g -factor is reduced by almost a factor 2. This result may reflect the g -factor anisotropy in Ge, even in this high doping regime. Indeed, in the Hanle configuration, electron spins precess by $\omega_L \tau_{sf} \approx 2\pi$ within the (001) crystal plane whereas they precess out of this plane by $\omega_L \tau_{sf} \approx 2\pi/3$ around the [110] crystal axis in the oblique Hanle configuration. This hypothesis clearly needs a theoretical support and additional measurements by varying the Ge substrate orientation from (100) to (110) and even (111) or by processing the ferromagnetic electrodes at different angles with respect to the applied field.

Finally, from the values of l_{sf} and NL magnetoresistance measurements, we use Eq. (1) to obtain: $P_I P_D \approx 0.0093$ at 10 K and $P_I P_D \approx 0.0724$ at 295 K. Assuming $P_I = P_D = \langle P \rangle$, we find: $\langle P \rangle \approx 10\%$ at 10 K and $\langle P \rangle \approx 27\%$ at 295 K showing the high spin injection efficiency using epitaxial MTJ on Ge. Surprisingly, the spin injection efficiency is systematically less at 10 K. A possible explanation is the existence of residual interface states at the MgO/Ge interface as discussed in Refs. 15 and 23. In this case, spin injection is a two-step tunneling process from the ferromagnetic layer to the Ge conduction band through the interface states. At low temperature (here 10 K), the transit time of electrons into the interface states may be comparable or longer than their spin lifetime. As a consequence, the spin accumulation into the Ge conduction band is reduced and the spin injection efficiency decreases. On the contrary, at room temperature, the transit time is much shorter and the two-step tunneling process has no more effect on the tunneling spin polarization restoring high spin injection efficiency. However, we cannot completely exclude a small dispersion in the MgO tunnel barrier quality from device to device that may also lead to some different spin injection efficiencies.

In summary, we have demonstrated spin transport in Ge at room temperature using non-local electrical detection and 3 different directions of the applied magnetic field. For this purpose, we used epitaxial Fe/MgO magnetic tunnel junctions to reach high spin injection efficiencies up to 27% at 295 K. We could give an accurate spin diffusion length of $1 \mu\text{m}$ at room temperature in heavily doped n -type Ge. Moreover, we have shown that the electron spin lifetime only decreases by a factor 1.5 between 10 K and 295 K revealing the dominant role of spin relaxation due to spin scattering on ionized dopants. Oblique Hanle measurements may reveal the g -factor anisotropy in Ge even in the high doping regime. Finally, those results definitely show that germanium spintronics has reached a high level of maturity.

The authors acknowledge the financial support from the French National Research Agency through the ANR project SiGeSPIN #ANR-13-BS10-0002. Dr. Edith Bellet-Amalric is also acknowledged for the x-ray diffraction analysis of GeOI.

¹D. D. Awschalom and M. E. Flatté, *Nat. Phys.* **3**, 153 (2007).

²I. Zutic, J. Fabian, and S. Das Sarma, *Rev. Mod. Phys.* **76**, 323 (2004).

³S. A. Wolf, D. D. Awschalom, R. A. Buhrman, J. M. Daughton, S. von Molnár, M. L. Roukes, A. Y. Chtchelkanova, and D. M. Treger, *Science* **294**, 1488–1495 (2001).

- ⁴F. Bottegoni, C. Zucchetti, S. Dal Conte, J. Frigerio, E. Carpena, C. Vergnaud, M. Jamet, G. Isella, F. Ciccacci, G. Cerullo *et al.*, *Phys. Rev. Lett.* **118**, 167402 (2017).
- ⁵C. Zucchetti, F. Bottegoni, C. Vergnaud, F. Ciccacci, G. Isella, L. Ghirardini, M. Celebrano, F. Rortais, A. Ferrari, A. Marty *et al.*, *Phys. Rev. B* **96**, 014403 (2017).
- ⁶P. Li, Y. Song, and H. Dery, *Phys. Rev. B* **86**, 085202 (2012).
- ⁷F. Bottegoni, G. Isella, S. Cecchi, and F. Ciccacci, *Appl. Phys. Lett.* **98**, 242107 (2011).
- ⁸Y. Zhou, W. Han, L.-T. Chang, F. Xiu, M. Wang, M. Oehme, I. A. Fischer, J. Schulze, R. K. Kawakami, and K. L. Wang, *Phys. Rev. B* **84**, 125323 (2011).
- ⁹L.-T. Chang, W. Han, Y. Zhou, J. Tang, I. A. Fischer, M. Oehme, J. Schulze, R. K. Kawakami, and K. L. Wang, *Semicond. Sci. Technol.* **28**, 015018 (2013).
- ¹⁰E.-S. Liu, J. Nah, K. M. Varahramyan, and E. Tutuc, *Nano Lett.* **10**, 3297 (2010).
- ¹¹P. Li, J. Li, L. Qing, H. Dery, and I. Appelbaum, *Phys. Rev. Lett.* **111**, 257204 (2013).
- ¹²A. Jain, L. Louahadj, J. Peiro, J.-C. Le Breton, C. Vergnaud, A. Barski, C. Beigné, L. Notin, A. Marty, V. Baltz *et al.*, *Appl. Phys. Lett.* **99**, 162102 (2011).
- ¹³H. Saito, S. Watanabe, Y. Mineno, S. Sharma, R. Jansen, S. Yuasa, and K. Ando, *Solid State Commun.* **151**, 1159 (2011).
- ¹⁴F. Rortais, S. Oyarzún, F. Bottegoni, J.-C. Rojas-Sánchez, P. Laczkowski, A. Ferrari, C. Vergnaud, C. Ducruet, C. Beigné, N. Reyren *et al.*, *J. Phys.: Condens. Matter* **28**, 165801 (2016).
- ¹⁵A. Jain, J.-C. Rojas-Sánchez, M. Cubukcu, J. Peiro, J. C. Le Breton, E. Prestat, C. Vergnaud, L. Louahadj, C. Portemont, C. Ducruet *et al.*, *Phys. Rev. Lett.* **109**, 106603 (2012).
- ¹⁶A. Jain, C. Vergnaud, J. Peiro, J.-C. Le Breton, E. Prestat, L. Louahadj, C. Portemont, C. Ducruet, V. Baltz, A. Marty *et al.*, *Appl. Phys. Lett.* **101**, 022402 (2012).
- ¹⁷K.-R. Jeon, B.-C. Min, Y.-H. Jo, H.-S. Lee, I.-J. Shin, C.-Y. Park, S.-Y. Park, and S.-C. Shin, *Phys. Rev. B* **84**, 165315 (2011).
- ¹⁸A. T. Hanbicki, S.-F. Cheng, R. Goswami, O. M. J. van 't Erve, and B. T. Jonker, *Solid State Commun.* **152**, 244 (2012).
- ¹⁹S. Iba, H. Saito, A. Spiesser, S. Watanabe, R. Jansen, S. Yuasa, and K. Ando, *Appl. Phys. Express* **5**, 053004 (2012).
- ²⁰S. Dushenko, M. Koike, Y. Ando, T. Shinjo, M. Myronov, and M. Shiraishi, *Phys. Rev. Lett.* **114**, 196602 (2015).
- ²¹V. Reboud, A. Gassenq, K. Guilloy, G. Osvaldo Dias, J. M. Escalante, S. Tardif, N. Pauc, J.-M. Hartmann, J. Widiez, E. Gomez *et al.*, *Proc. SPIE* **9752**, 97520F (2016).
- ²²A. Fert and H. Jaffrès, *Phys. Rev. B* **64**, 184420 (2001).
- ²³M. Tran, H. Jaffrès, C. Deranlot, J.-M. George, A. Fert, A. Miard, and A. Lemaître, *Phys. Rev. Lett.* **102**, 036601 (2009).
- ²⁴Y. Song and H. Dery, *Phys. Rev. Lett.* **113**, 047205 (2014).
- ²⁵O. Txoperena, Y. Song, L. Qing, M. Gobbi, L. E. Hueso, H. Dery, and F. Casanova, *Phys. Rev. Lett.* **113**, 146601 (2014).
- ²⁶T. Sasaki, T. Oikawa, T. Suzuki, M. Shiraishi, Y. Suzuki, and K. Noguchi, *Appl. Phys. Lett.* **98**, 262503 (2011).
- ²⁷F. J. Jedema, H. B. Heersche, A. T. Filip, J. J. A. Baselmans, and B. J. van Wees, *Nature* **416**, 713 (2002).
- ²⁸J.-C. Rojas Sánchez, P. Laczkowski, W. F. Savero Torres, M. Cubukcu, V. D. Nguyen, L. Notin, C. Beigné, C. Vergnaud, A. Marty, M. Jamet *et al.*, *Appl. Phys. Lett.* **102**, 132408 (2013).
- ²⁹Y. Fukuma, L. Wang, H. Idzuchi, S. Takahashi, S. Maekawa, and Y. Otani, *Nat. Mater.* **10**, 527 (2011).
- ³⁰G. Feher, D. K. Wilson, and E. A. Gere, *Phys. Rev. Lett.* **3**, 25 (1959).
- ³¹Y. Song, O. Chalaev, and H. Dery, *Phys. Rev. Lett.* **113**, 167201 (2014).
- ³²Y. Fujita, M. Yamada, S. Yamada, T. Kanashima, K. Sawano, and K. Hamaya, *Phys. Rev. B* **94**, 245302 (2016).
- ³³J.-N. Chazalviel, *J. Phys. Chem. Solids* **36**, 387 (1975).
- ³⁴M. V. Fischetti, *IEEE Trans. Electron Devices* **38**, 634 (1991).